Giant in-plane magnetic anisotropy in epitaxial bcc Co/Fe(110) bilayers

M. Ślęzak,[1,2,*] T. Ślęzak,[1] K. Matlak,[1] B. Matlak,[1] P. Dróżdż,[1] T. Giela,[3] D. Wilgocka-Ślęzak,[3]
N. Pilet,[2] J. Raabe,[2] A. Kozioł-Rachwał,[1,4] and J. Korecki[1,3]
[1]*Faculty of Physics and Applied Computer Science, AGH, Kraków, Poland*
[2]*Swiss Light Source, Paul Scherrer Institut, Villigen, Switzerland*
[3]*Jerzy Haber Institute of Catalysis and Surface Chemistry PAS, Kraków, Poland*
[4]*National Institute of Advanced Industrial Science and Technology, Spintronics Research Center, Tsukuba, Ibaraki 305-8568, Japan*
(Received 11 March 2016; revised manuscript received 25 May 2016; published 5 July 2016)

We report on in-plane magnetic anisotropy in epitaxial bcc Co/Fe(110) bilayers on W(110). The magnetic surface anisotropy in the Co/Fe(110) bilayers exhibited a strong nonmonotonic dependence on Co coverage. Magneto-optical studies revealed a sharp maximum of the magnetic surface anisotropy, 2.44 mJ/m^2, at $d_{\mathrm{Co}} = 5$ Å. This giant interfacial magnetic anisotropy allowed a small fraction of a Co monolayer to reorient the magnetization of the bulk-like Fe film. We conclude that the mono- and double-layer bcc Co(110) exhibited in-plane magnetic anisotropy with a [1$\bar{1}$0] easy axis.

DOI: 10.1103/PhysRevB.94.014402

I. INTRODUCTION

A key characteristic of magnetic materials is their magnetic anisotropy (MA). A material's MA determines its direction of spontaneous magnetization, which must be precisely controlled in order to use the material in applications such as data storage and sensors. In low-dimensional magnetic systems, such as thin films, important contributions beyond volume magnetocrystalline anisotropy should be considered, such as shape, surface/interface, and magnetoelastic anisotropy. The effective MA of a thin ferromagnetic (FM) film is related to spin reorientation transition (SRT) phenomena [1], which can be usually tuned by changing the balance between contributions from the thickness and from temperature-dependent volume and surface (interface) anisotropy [1,2]. Another way to control the MA of a thin film is to directly alter its interface or surface anisotropy. The latter method is usually attempted by gas adsorption on the film surface [3] or by deposition of both magnetic [4] and nonmagnetic [5] capping materials.

Weber *et al.* demonstrated a convincing example of this kind of spin engineering for a Co film on Cu(100) [5], showing that depositing a Cu layer as thin as 0.03 monolayers (ML) was sufficient to rotate the spins of the 20-ML-thick Co film by 90°. Similarly, the magnetization of a ferromagnetic film can be easily switched in any system near the SRT. One of the first SRTs was observed in Fe(110)/W(110) films [6,7], where the magnetization switched from the [1$\bar{1}$0] to the [001] in-plane direction while growing the Fe film when its thickness approached a critical value. The critical thickness of this SRT can be tuned in the range of 100 ± 50 Å, depending on the preparation conditions of the Fe film [8] and by depositing noble metal (Ag, Au) adlayers [9,10]; adsorption of oxygen [9] and even ultra-high-vacuum (UHV) residual gases can drive the in-plane rotation of Fe magnetization.

In the present report, we show that capping epitaxial Fe(110) films, grown on W(110), with a bcc-Co overlayer greatly changes their in-plane magnetic surface anisotropy (MSA). Accordingly, we induced a 90° in-plane reorientation in the magnetization of a 13-nm-thick Fe film from the [001] bulk easy magnetization direction to [1$\bar{1}$0] by depositing a fraction of a Co monolayer. With increasing Co thickness, the Co/Fe magnetic anisotropy evolves nonmonotonically.

II. GROWTH AND STRUCTURE

The *in situ* structural and magnetic properties of MBE-grown epitaxial Co/Fe(110)/W(110) samples were analyzed. The Fe(110) films with a thickness of several nanometers to several tens of nanometers were grown on atomically clean W(110) single crystal at room temperature and then annealed at 675 K. This produced high-quality epitaxial Fe films with atomically smooth (110) surfaces, consistent with the literature [10]. Next, on the Fe(110) film, a wedge-shaped Co adlayer with a thickness continuously increasing from zero to several tens of angstroms was deposited at room temperature. After each processing step the structure of the surface was monitored using low-energy electron diffraction (LEED).

Figure 1(a) shows LEED patterns from the surfaces of the Fe(110)/W and Co/Fe(110)/W(110) wedges for selected Co thicknesses. The (1 × 1) diffraction patterns corresponding to a Co thickness of $d_{\mathrm{Co}} \leqslant 5$ Å indicate pseudomorphic growth of Co on the Fe(110) surface. For thicker Co films, characteristic superstructure spots appeared as a result of the periodic lattice distortion existing in two equivalent (3 × 1) reconstruction domains. A similar structure has been reported for Co on a Cr(110) surface [11] isostructural with the Fe(110) plane. Following the careful analysis of Fölsch *et al.* [11], we conclude that our LEED patterns correspond to the bcc Co(110) structure; however, the reconstructed film surface appears beyond the second Co monolayer.

In Fig. 1(b) we present the thickness dependence of the in plane lattice spacing a_{001} along the Fe[001] direction for the Co film, as determined from the LEED patterns. At the surface of a 200 Å thick Fe film we found $a_{001}^{\mathrm{Fe}} = 2.89 \pm 0.02$ Å which corresponds to a not-fully-relaxed Fe(110)/W film when compared to 2.86 Å for bulk iron. Within the accuracy of our method, in the 0–25 Å thickness range Co exhibits the same in plane lattice constant as Fe(110) surface. Moreover, the (1 × 1) LEED patterns for Co thickness less than ∼6 Å indicate pseudomorphic growth. For thicker Co films the (3 × 1) reconstruction appears, and eventually the LEED patterns

*mislezak@agh.edu.pl

 ©2016 American Physical Society

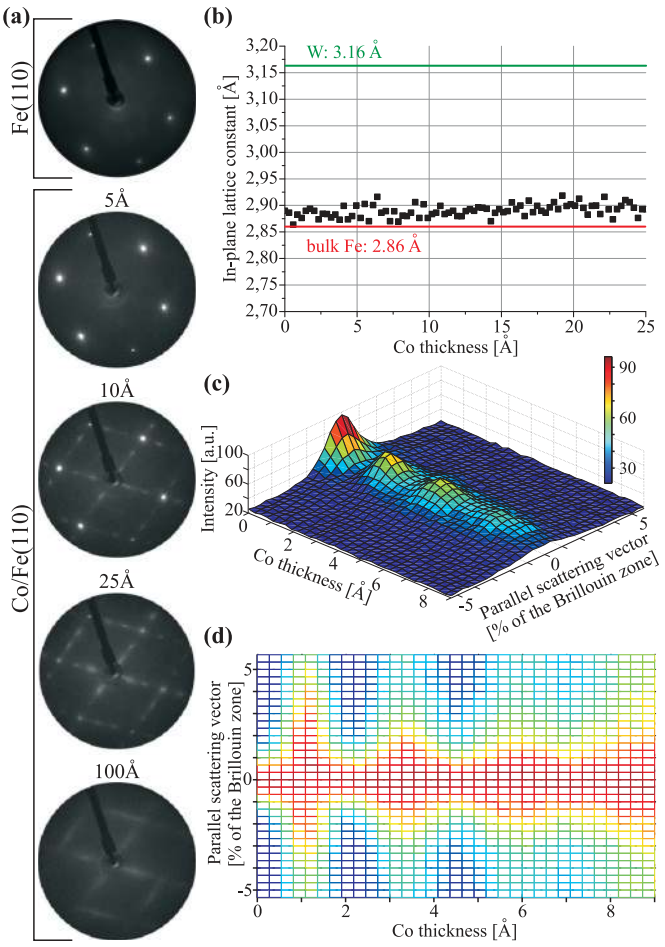

FIG. 1. **(a)** LEED patterns ($E = 120$ eV) from Fe(110) and from bcc Co films with thicknesses of 5, 10, 25, and 100 Å on Fe(110), **(b)** thickness dependence of in-plane lattice constant for bcc Co/Fe(110) as determined from LEED spots positions, **(c)** 3D visualization of the (01) LEED spot profile in the ⟨001⟩ azimuth as a function of Co film thickness. Colors blue-red (color online) correspond to the 0–100 intensity range in arbitrary units. **(d)** The top view of (c) after normalization of intensity in each spot profile is shown.

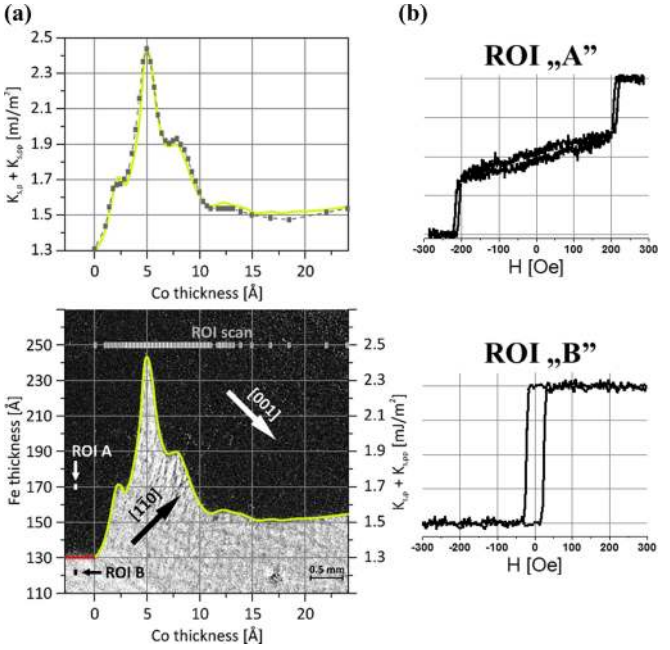

FIG. 2. **(a)** (Lower panel) Differential MOKE image of the surface (crystal diameter = 8 mm; presented field of view =∼ 4.5 × 4.5 mm^2) taken in the sample's remanence state after saturation in a magnetic field parallel to the [1$\bar{1}$0] in-plane direction. The green line shows the dependence of Fe thickness, at which the SRT takes place, on Co thickness. (Upper panel) MSA as a function of Co thickness, extracted from hysteresis loops measured from scans of the regions of interest (ROIs) marked in the lower panel. For comparison, the SRT border (solid line) from the MOKE image is also repeated here. **(b)** Two exemplary hysteresis loops characteristic of the dark (ROI "A") and bright (ROI "B") areas of the image shown in (a).

become blurred, which makes the further evaluation of lattice constant ambiguous.

In Fig. 1(c) we present the 3D visualization of the evolution of the (01) LEED spot profile with increasing Co thickness. The maxima of the spot profile intensity occur with roughly 2 Å (1 ML) period and should be related to completion of subsequent Co monolayers. On the other hand, for each incomplete Co monolayer (increased roughness) we observe a maximum of the LEED spot width, as seen in Fig. 1(d) where we present the top view of Fig. 1(c) after normalization of intensity in each spot profile. The presented evolution of the intensity and width of the (01) LEED spot indicates a close to layer-by-layer growth mode of Co on Fe(110). For thicker Co films the oscillations of intensity and width of the LEED spot profiles disappear. In LEED patterns it is accompanied by the onset of already mentioned superstructure caused by periodic lattice distortions. We associate this structural transformation with a change from flat to three dimensional growth mode of Co on Fe(110).

III. MAGNETIC PROPERTIES

The magnetic properties of the Co/Fe(110)/W(110) system were imaged *in situ*, by using the longitudinal magneto-optic Kerr effect (MOKE), as a function of the Co and Fe thicknesses. For this purpose, we grew a double-wedge sample, with two orthogonal wedges of Co and Fe, according to the process described earlier. The thicknesses of the Fe (d_{Fe}) and Co (d_{Co}) wedges were continuously varied from 90 to 300 Å and from 0 to 30 Å, respectively.

The lower panel of Fig. 2(a) shows a differential MOKE image of a selected area of the double-wedge Co/Fe(110) sample. To enhance the magnetic contrast, we subtracted a reference image taken at saturation in an external magnetic field along [1$\bar{1}$0] from the image taken at remanence. Consequently, the bright area is where the remanence magnetization remained along the saturation direction, [1$\bar{1}$0], whereas the dark area corresponds to the [001] magnetization direction in the remanent state. The border between them, shown by the green line, visualizes the in-plane SRT in the (d_{Fe}, d_{Co}) space, and its shape reflects an oscillatory dependence of SRT (and hence the effective MSA) on the Co thickness. Furthermore, the Co-coated films exhibited a clear increase in Fe critical thickness $d_c(d_{Co})$, compared with the uncoated Fe film ($d_c = 130$ Å as shown by the horizontal red line in Fig. 2[a]), across the entire range of Co thickness. This

enhancement was greatest at $d_{Co} \approx 5$ Å, where the critical Fe thickness increased by ~90% to 244 Å.

We analyzed the thickness dependence of MA in the bcc Co(110)/Fe(110) films by examining a series of MOKE images taken as a function of external magnetic field H applied along the $[1\bar{1}0]$ in-plane direction. The magnetic hysteresis loops can be extracted for any combination of Co and Fe thicknesses by choosing a sample region of interest (ROI), which can be as small as one pixel. The typical size of a ROI was $90 \times 50\,\mu m^2$, which corresponds to the average over the finite thickness differences of 2.5 Å and 0.15 Å for the Fe and Co wedges, respectively. Figure 2(b) shows two hysteresis loops representative of the dark (ROI "A") and bright (ROI "B") areas of the image. The square hysteresis loops measured from the bright area and the typical hard loops corresponding to the dark area confirm that the green line in Fig. 2(a) marks the SRT border. The almost hysteresis-less hard-axis loops with the characteristic magnetization switching at the saturating field can be fitted by minimization of the free enthalpy density G as a function of the external magnetic field H:

$$G = A\sin^2(\theta) + B\sin^4(\theta) - M_s H\sin(\theta), \quad (1)$$

where M_s is the saturation magnetization, θ defines the orientation of magnetization with respect to the [001] in-plane direction, and A and B are the second- and fourth-order effective magnetic anisotropy constants.

First, we determined the effective anisotropy constants for the uncoated Fe(110) film by choosing the ROIs in Fig. 2(a) with no Co. The effective anisotropy constants were interpreted in terms of the volume and surface magnetic anisotropies [10]: $A = K_{v,p} - K_{s,p}/d_{Fe}$ and $B = K_{v,pp} - K_{s,pp}/d_{Fe}$, where $K_{v,p}$ and $K_{v,pp}$ are the second- and fourth-order volume constants of in-plane magnetic anisotropy, with $K_{s,p}$ and $K_{s,pp}$ denoting their surface analogues. From the linear dependence of A and B on the inverse Fe thickness, we determined the volume and surface in-plane magnetic anisotropy constants for our Fe(110) films. We find $K_{v,p} = 10.60^{*}10^4\,J/m^3$ and $K_{s,p} = 0.82\,mJ/m^2$, which agree well with reported data [10], and $K_{v,pp} = -0.60^{*}10^4\,J/m^3$ and $K_{s,pp} = 0.48\,mJ/m^2$, which are very different from those reported by Elmers and Gradmann [10], especially the opposite sign of their $K_{s,pp}$, $-0.16\,mJ/m^2$, suggesting that it is very sensitive to film structure and morphology.

Now we focus on the results for 5-Å Co/Fe(110), which exhibited the strongest influence of Co on the Fe critical thickness. Analyzing hysteresis loops as a function of Fe thickness yielded $K_{v,p}$ and $K_{v,pp}$ values very similar to those of uncoated Fe(110); however, the total MSA energies $(K_{s,p} + K_{s,pp})$ greatly increased from 1.30 in uncoated Fe(110) to $2.44\,mJ/m^2$ in 5-Å Co/Fe(110). We conclude that the Co overlayer mainly influences the surface magnetic anisotropy of the Fe(110) film.

With the above analysis, the green line in Fig. 2(a) can be interpreted as indicating the cancelation of the in-plane effective magnetic anisotropy of Co/Fe(110) at the critical Fe thickness d_c : $K_{s,p} + K_{s,pp} = (K_{v,pp} + K_{v,p})d_c$. Using the values of $K_{v,p}$ and $K_{v,pp}$ derived for uncovered Fe(110), we rescaled the d_c values to the total MSA (right scale in Fig. 2[a]), which explicitly shows the nonmonotonic dependence of the MSA on Co thickness. Such a simplified analysis of MSA is further supported by a more detailed analysis of the hysteresis loops measured along the Co wedge at $d_{Fe} = 250$ Å; see "ROI scan" in the MOKE image in the Fig. 2(a). The resulting $(K_{s,p} + K_{s,pp})$ values of MSA are plotted versus d_{Co} in the upper panel of Fig. 2(a) (dots with dashed line), together with the dependence directly seen in the differential MOKE image below (solid line). The MSA values derived from these two independent analyses agree perfectly. Note also that the shape of the MSA dependence on Co thickness was reproduced in several samples.

The most interesting and striking effect in Fig. 2(a) is the huge increase of in-plane MSA in the Fe/Co bilayers over the Co thickness range of 0–5 Å. At Co coverage of up to one monolayer, we interpret this behavior as a strong modification of the Fe(110) MSA caused by the Co adatoms. Then, in the range of $\sim 2.5 - 5.0$ Å, an even steeper increase of MSA appeared, which likely comes from the onset of inherent magnetic anisotropy in the bcc Co(110) adlayer, evidently preferring the $[1\bar{1}0]$ easy axis. No experimental data has been reported on the magnetic anisotropy of such ultrathin bcc Co(110) films. The available calculations of MA in mono- and double-layers bcc-Co(110) films [12] suggest that MA depends very strongly on thickness and do not contradict our conclusion that our ultrathin bcc-Co(110) films have a $[1\bar{1}0]$ easy axis.

The second distinct feature in Fig. 2(a) is the drastic decrease in the Fe/Co bilayer MSA over the Co thickness range of 5–10 Å. This behavior roughly coincides with the onset of additional superstructure visible in the LEED patterns at Co thicknesses above 5 Å, indicating that the structural transformation in the Co adlayer reduced the strength of the $[1\bar{1}0]$-type MA at the Fe/Co interface. An alternative explanation assumes that the in-plane easy axis of the inherent Co magnetic anisotropy switched from $[1\bar{1}0]$ to [001]. It would not be surprising if, over this thickness range, the easy axis in bcc Co films was [001]: this result has been reported in 6.5- and 9-ML-thick bcc-Co films on Cr(110) [13] and 357-Å-thick Co on GaAs(110) [14]. However, for sufficiently thick Co films, this should cause a drop of the green line in Fig. 2 below that for the uncovered Fe(110) surface. We exclude this possibility for the studied Co thickness range of 0–100 Å.

Now we will comment on the third effect, the short-period oscillations visible in the $d_c(d_{Co})$ dependence shown in Fig. 2(a). Following the interpretation by Weber *et al.* of similar periodicity observed in Co films on Cu(001) [15], we attribute the oscillations to periodic alterations of the Co surface morphology between incomplete and filled atomic layers. The deviation from the ideal layer-by-layer growth of Co on Fe(110) explains why the period of these oscillations only roughly corresponds to 1 ML. This interpretation is strongly supported by the analysis of the LEED spot profiles presented in Figs. 1(c) and 1(d). The local maxima of the SRT critical thickness and Co/Fe MSA roughly correspond to the positions of the maxima in Fig. 1(c) and minima in Fig. 1(d). The good agreement between the oscillations of structural and magnetic properties supports our interpretation of the morphology-induced oscillations of MSA in the Co/Fe(110) bilayers.

Our analysis assumes the presence of ferromagnetic exchange coupling between the Fe(110) film and the Co adlayer for all Co and Fe thicknesses. We studied the Fe–Co exchange

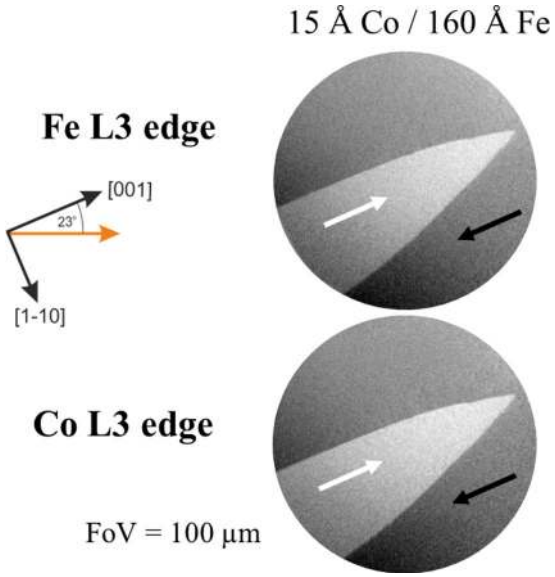

FIG. 3. XMCD-PEEM images of the domain structures in the Fe (upper panel) and Co (lower panel) sublayers in Co(15 Å)/Fe(110)/W(110). The left inset defines the orientation of the sample with respect to the incident x rays. The arrows in the XMCD-PEEM images show the magnetization directions in the corresponding magnetic domains.

coupling by using x-ray magnetic circular dichroism (XMCD) in a photoemission electron microscope (PEEM) temporarily installed [16,17] at the NanoXAS beamline [18] in Swiss Light Source.

Figure 3 shows representative XMCD-PEEM images of the 15-Å-thick Co adlayer on 160-Å Fe(110)/W(110), acquired at the L3 edge of Fe (upper panel) or Co (lower panel). White–white and dark–dark intensity correlations, corresponding to the Fe and Co magnetic domains, appeared over the whole range of investigated Fe and Co film thicknesses, and indicate ferromagnetic Fe–Co magnetic coupling.

IV. CONCLUSIONS

In conclusion, we found a very strong nonmonotonic dependence of the Co/Fe magnetic surface anisotropy on the thickness of the Co overlayer. The Co adlayers increased the MSA from 1.30 mJ/m^2 for the uncovered Fe(110) surface to 2.44 mJ/m^2 for the Co(5 Å)/Fe(110) bilayer. We compare this 1.14 mJ/m^2 (corresponding to 0.41 meV/atom) increase in MSA induced by Co to the much smaller modifications in MSA reported for nonmagnetic overlayers on Fe(110), in which Cu and Ag changed the MSA by 0.07 mJ/m^2(∼0.03 meV/atom) and 0.11 mJ/m^2 (0.04 meV/atom), respectively [10]. The MSA reported here for Fe(110)/Co(110) interface is much higher than any others reported for FM/FM interfaces [19]. Such exceptionally high MSA allows a small fraction of a Co monolayer to govern the magnetization of a relatively thick bulk-like Fe film. Apart from these huge modifications in MSA induced by Co at the all-bcc Co(110)/Fe(110) interface, our results reveal $[1\bar{1}0]$ in-plane MA in the mono- and double-layers of bcc-Co(110).

ACKNOWLEDGMENTS

The PEEM project was funded by EU European Regional Development Fund, OP IE 2007-2013. This work was supported in part by the Scientific Exchange Programme NMS-CH (SCIEX) project, by the TEAM Program of the Foundation for Polish Science (co-financed by the EU European Regional Development Fund), and the Marian Smoluchowski Krakow Research Consortium (the Leading National Research Centre, KNOW, which is supported by the Polish Ministry of Science and Higher Education).

Invaluable help of many colleagues from PSI, especially F. Nolting, A. Kleibert, P. Warnicke, and B. Sarafimov, in installation and running of Polish PEEM at SLS is gratefully acknowledged.

[1] Y. Millev and J. Kirschner, Phys. Rev. B **54**, 4137 (1996).
[2] H. P. Oepen, M. Speckmann, Y. Millev, and J. Kirschner. Phys. Rev. B **55**, 2752 (1997).
[3] S. Hope, E. Gu, B. Choi, and J.A.C. Bland, Phys. Rev. Lett. **80**, 1750 (1998).
[4] J. Shen, A. K. Swan, and J. F. Wendelken, Appl. Phys. Lett. **75**, 2987 (1999).
[5] W. Weber, C. H. Back, A. Bischof, D. Pescia, and R. Allenspach, Nature **374**, 788 (1995).
[6] U. Gradmann, J. Korecki, and G. Waller, Appl. Phys. A **39**, 101 (1986).
[7] T. Ślęzak, M. Ślęzak, M. Zając, K. Freindl, A. Kozioł-Rachwał, K. Matlak, N. Spiridis, D. Wilgocka-Ślęzak, E. Partyka-Jankowska, M. Rennhofer, A. I. Chumakov, S. Stankov, R. Rüffer, and J. Korecki, Phys. Rev. Lett. **105**, 027206 (2010).
[8] M. Albrecht, T. Furubayashi, M. Przybylski, J. Korecki, and U. Gradmann, J. Magn. Magn. Mater. **113**, 207 (1992).
[9] I. G. Baek, H. G. Lee, H. J. Kim, and E. Vescovo, Phys. Rev. B **67**, 075401 (2003).
[10] H. J. Elmers and U. Gradmann, Appl. Phys. A **51**, 255 (1990).
[11] S. Fölsch, A. Helms, A. Steidinger, and K. H. Rieder, Phys. Rev. B **57**, R4293 (1998).
[12] J. Dorantes-Dávila and G. M. Pastor, Phys. Rev. Lett. **77**, 4450 (1996).
[13] S. Fölsch, A. Helms, A. Steidinger, and K. H. Rieder, J. Magn. Magn. Mater. **191**, 38 (1999).
[14] G. A. Prinz, Phys. Rev. Lett. **54**, 1051 (1985).
[15] W. Weber, C. H. Back, A. Bischof, Ch. Würsch, and R. Allenspach, Phys. Rev. Lett. **76**, 1940 (1996).
[16] M. Ślęzak, T. Giela, D. Wilgocka-Ślęzak, A. Kozioł-Rachwał, T. Ślęzak, R. Zdyb, N. Spiridis, C. Quitmann, J. Raabe, N. Pilet, and J. Korecki, J. Magn. Magn. Mater. **348**, 101 (2013).
[17] M. Ślęzak, T. Giela, D. Wilgocka-Ślęzak, N. Spiridis, T. Ślęzak, M. Zając, A. Kozioł-Rachwał, R. P. Socha, M. Stankiewicz, P. Warnicke, N. Pilet, J. Raabe, C. Quitmann, and J. Korecki, X-Ray Spectrometry **44**, 317 (2015).
[18] N. Pilet, J. Raabe, S. E. Stevenson, S. Romer, L. Bernard, C. R. McNeill, R. H. Fink, H. J. Hug, and C. Quitmann, Nanotechnology **23**, 475708 (2012).
[19] M. T. Johnson, P. J. H. Bloemen, F. J. A. den Broeder, and J. J. de Vries, Rep. Prog. Phys. **59**, 1409 (1996).